Arch. Metall. Mater. **70** (2025), 2, 715-720

DOI: https://doi.org/10.24425/amm.2025.153472

A. WÓJCIK[1*], R. CHULIST[1], A. SZEWCZYK[1], B. MOROŃCZYK[2,3], Ł. ŻRODOWSKI[2,3], R. WRÓBLEWSKI[2], M. KOWALCZYK[2] W. MAZIARZ[1]

MICROSTRUCTURAL CHARACTERIZATION OF 3D PRINTED NIMNGACoCu BASED MAGNETIC SHAPE MEMORY ALLOYS

The main aim of this research was to produce, by laser powder bed fusion (LPBF) process, good quality material with non-modulated martensite structure exhibiting high magnetic field-induced strain value. The microstructure and texture of NiMnGaCoCu alloy were investigated by SEM, TEM, and high-energy X-ray diffraction. It was shown that LPBF process combined with the post-processing annealing allowed to obtain a homogeneous microstructure with a strong <100> fiber texture along the growth direction. It was also shown that the scanning strategy does not greatly affect the microstructure and crystal structure of the material while the only difference lies in the existence of a double texture component for alloy produced by oscillating mode. Finally, the magnetic field-induced strain value calculated for the alloy with non-modulated martensite produced by the 3D printing was about 0.2%.

Keywords: Ni-Mn-Ga ferromagnetic shape memory alloys; additive manufacturing; microstructure; texture; MFIS

1. Introduction

Additive manufacturing (AM) technologies, called 3D printing, have gained much scientific, public, and commercial interest for the last three decades showing a strong alternative to conventional fabrication techniques [1-5]. AM provides many advantages such as (i) fabrication of complicated and complex geometries in one piece including thin walls and small holes (ii) the ability to print a wide range of materials (including metals, ceramics, polymers and even composites), (iii) reduced manufacturing costs and lead times while the cost saving rises when the part shows more complex shapes, (iv) tailoring the processing conditions allowing to produce desire shapes, dimensions etc. However, here, the drawbacks and challenges should also be reminisced. Firstly, AM has not been considered as a completely viable process yet, especially when compared with other conventional processes. Secondly, the produced pieces of materials, more often, do not show sufficient precision while there are some limitations in the surface finish. Moreover, the fast cooling rates during the process introduce stresses and distortions to the materials providing structural defects. Taking into account feedstock, energy source, and build volume, the metal AM technologies can be divided into three main groups: (i) powder bed systems, (ii) powder feed systems and (iii) wire feed systems [5] creating new possibilities and solutions for many types of functional materials. AM methods combined with the proper heat treatment can be successfully applied to produce Ni-Mn-Ga ferromagnetic shape memory alloys allowing to control of not only the shape of the alloys but also chemical composition, microstructure and texture, which in fact, determine the functional properties such as magnetic field induced strain (MFIS) values and working temperature [6-9]. Ni-Mn-Ga-based alloys belong to the group of so-called smart materials that can change their shape when changing temperature, magnetic field or applied stress. The abovementioned properties are related to thermoelastic martensitic transformation occurring in these alloys [10-16]. The martensitic transformation behavior can be tailored by chemical composition, microstructural features and atomic order degree. These are often associated with the manufacturing process and heat treatment. Thus, one of the most important issues is to design the chemical composition leading to obtain different martensite structures at room temperature (non-modulated, ten-layered (10M) and fourteen-layered (14M) structures) while the second one is to obtain the favorable microstructure and texture [17-22]. These would ensure the optimal conditions for MFIS in polycrystalline material.

[1] INSTITUTE OF METALLURGY AND MATERIALS SCIENCE, POLISH ACADEMY OF SCIENCES, 25 REYMONTA STR., 30-059 KRAKÓW, POLAND
[2] WARSAW UNIVERSITY OF TECHNOLOGY, FACULTY OF MATERIALS SCIENCE AND ENGINEERING, 141 WOŁOSKA STR., 02-507 WARSAW, POLAND
[3] AMAZEMET SP. Z O.O., AL. JANA PAWŁA II 27, 00-867 WARSAW, POLAND

* Corresponding author: anwojcik@agh.edu.pl

In this work, we have investigated NiMnGaCoCu alloys fabricated by the Laser Powder Bed Fusion technique using two different scanning strategies that may affect the final product quality and its microstructural features. The microstructural investigation was carried out using high energy X-ray diffraction and electron microscopy while MFIS value was calculated based on global texture measurements, and finally, martensitic transformation temperatures were determined by Physical Properties Materials System.

2. Experimental details

The powder precursor with irregular, non-spherical shapes and an average particle size of 15.2 ± 4.4 μm was prepared via milling of melt-spun ribbons, with the nominal composition of $Ni_{47}Mn_{25.5}Ga_{21.5}Co_3Cu_3$, in a vibration mill under 1 mm vibration amplitude for 2 h. The detailed procedures concerning both ribbons and powders production were described in Ref. [23-25]. Then, the alloys were built by Laser Powder Bed Fusion (LPBF) technique using a single-line strategy with two sub-strategies called normal (N) and oscillating (O). The main difference between both sub-strategies lies mainly in the scanning vector length and direction. And so, in the first case, the laser goes from the starting to the end point along a straight line whereas in the second case the laser moves in a zigzag manner. Moreover, the following process parameters: 37.5 W of laser beam power, laser beam diameter of 50 μm, and laser scanning speed of 250 mm/s were used. For more details see [26]. The 3D printings were subjected to annealing at 300, 600, 900°C for 1 h and at 900°C for 24 h and 72 h in an argon atmosphere followed by air cooling. The structure, phase composition, and global texture were examined by high-energy X-ray diffraction measurements at DESY in Germany, Hamburg, using the beamline P07B (87.1 keV, λ = 0.0142342 nm) [26,27]. Microstructural observations were carried out by FEI Quanta 3D field emission gun scanning electron microscope (SEM) equipped with Trident energy-dispersive X-ray spectrometer (EDX) produced by EDAX and TSL electron backscattered diffraction (EBSD) system as well as Tecnai G2 Transmission Electron Microscope (TEM) equipped with energy dispersive X-ray microanalyzer (EDX). The characteristic martensitic and magnetic transformation temperatures were examined by Physical Properties Materials System (PPMS) with VSM mode. The field cooling and field heating curves were recorded under magnetic field of about 500 Oe. Samples for SEM observations were mechanically polished and then etched electrolytically at room temperature with a Struers electropolishing LectroPol-5 using an electrolyte of nitric acid (vol. 1/3) and methanol (vol. 2/3). Thin foils for TEM were prepared with TenuPol-5 double jet electropolisher using also an electrolyte of nitric acid (vol. 1/3) and methanol (vol. 2/3) at a temperature near –25°C.

3. Results and discussion

The materials in the form of elongated plates with a length of 30-50 mm and width of 5 mm were produced via the LPBF process (see the inset of Fig. 1). The microstructural observations were performed on the surface marked by the red square. Fig. 1 presents the backscattered electron BSE SEM images revealing the microstructure of both samples (N and O) which is composed of columnar grains with a width between 70-100 μm, independently of the scanning strategy. It is well known that the grain growth direction is related to heat transfer during the 3D printing process (marked by red arrow) being perpendicular to the printing platform. Whereas, the small deviations of columnar grains of about 15-20° from the growth direction towards the laser vector direction are visible for both samples. This effect is related to the direction of laser movement and it depends on the printing speed. Columnar grains for N sample are deviated only in one direction while for O sample for two directions which

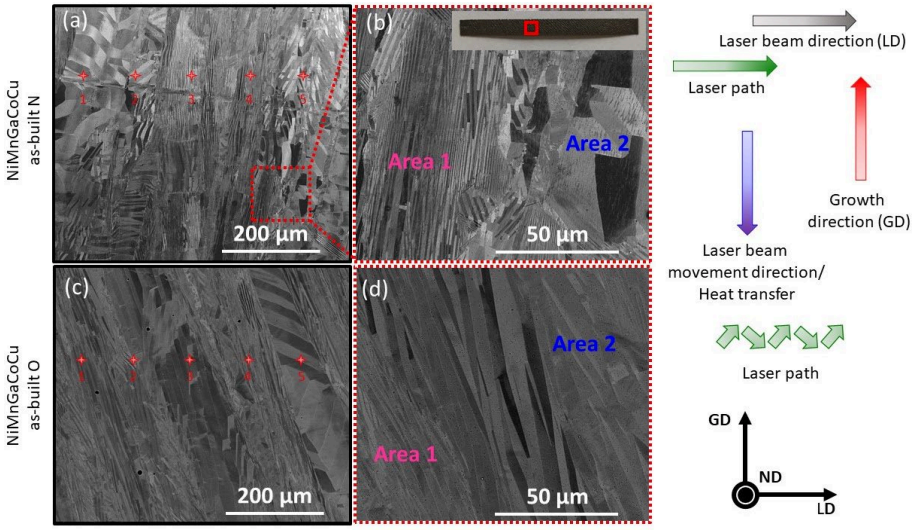

Fig. 1. BSE SEM images of as-built N (a), (b) and O (c), (d) samples taken with different magnifications. GD is growth direction, ND is normal direction, LD is laser direction

is related to the scanning strategy. Moreover, interestingly, in both cases, N and O samples two different regions/areas can be distinguished. Area 1 is composed of larger colonies with fine elongated martensite plates arranged in the direction of growth/heat transfer while in Area 2 wider plates are visible. Both BSE and EBSD measurements along with pole figures allowed to characterize both regions (Fig. 2).

The image clearly shows two areas separated by distinct boundaries, marked by a white dotted line. Area 1, is characterized by thinner martensite plates with an average width of a few μm while Area 2 is composed of wide twins with a size from 10-40 μm. Moreover, inside of the coarser martensite plates, there are some finer in size twins. Interestingly, the twins inside of the wider plates are finer (a few nm) compared to those that occurred in Area 2 (dozen of nm). The (001) pole figures recorded from both regions are depicted in Fig. 2. The texture of Area 2 (blue in Fig. 2) can be determined as the {001}<100> cube with (001) being slightly rotated from GD and LD. On the other hand, area 1 (pink in Fig. 2) with much broader macro twins and finer nano twins exhibits a rotated cube component. These orientations are rotated about 45° about GD indicating some variant selection during columnar grain growth. Nevertheless, both components account for a <100> fiber texture and are mainly related to the 3D printing process during which the molten alloy is dragged by laser.

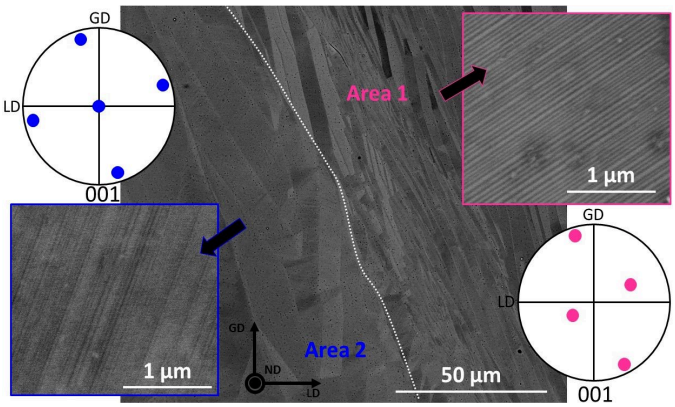

Fig. 2. BSE SEM images of NiMnGaCoCu O sample with pole figures recorded from both areas

Fig. 3 shows EBSD phase maps for NiMnGaCoCu N sample in as-built (a) and annealed (b) state. Based on the EBSD images two regions are also visible for both samples after 3D printing and annealing. IPF color coding maps indicate different colonies distribution, their orientation and twin arrangement as demonstrated above. Additionally, the orientations maps show a large number of finer and less regular twins for the as-built state while more uniformly distributed colonies and twin structures can be seen in the annealed sample.

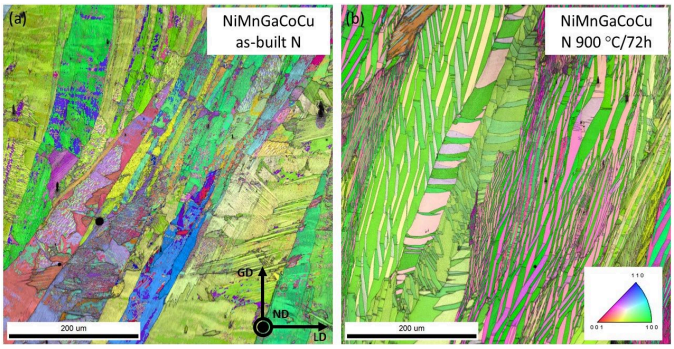

Fig. 3. IPF EBSD maps for NiMnGaCoCu N in as-built state (a) and annealed at 900°C/72 h

Moreover, the chemical composition of both samples has been examined by SEM EDS. The point analysis was taken from points marked by red stars in Fig. 1 and the results are listed in TABLE 1. Both samples were homogenous along the entire length with only small, almost neglected differences between marked points. However, it should be mentioned that there is a significant difference in Mn concentration between nominal and experimental/measured chemical compositions being related to intense Mn evaporation caused by double remelting firstly during melt spinning and secondly during LPBF processes. Interestingly, the O laser path leads to additional remelting of the material when the laser goes forward and backward in a zigzag way, thus, the sample shows slightly lower Mn concentration with respect to the N one.

Yet despite Mn depletion in both samples, the desired structure of non-modulated (NM) martensite was found for both N

TABLE 1

Results of EDS SEM analysis taken from points marked by red stars in Fig. 1, average chemical compositions and standard deviations for both N and O as-built samples

Sample	Element	1	2	3	4	5	Avg.	Std. dev.	e/a
as-built N	Ni(K) at.%	49.2	48.9	48.5	48.8	48.5	48.8	0.3	7.828
	Mn(K) at.%	23.2	23.3	23.7	23.3	23.9	23.5	0.3	
	Ga(K) at.%	20.9	21.2	20.8	21.2	20.9	21.0	0.2	
	Co(K) at.%	3.3	3.2	3.3	3.1	3.3	3.2	0.1	
	Cu(K) at.%	3.4	3.4	3.7	3.6	3.4	3.5	0.1	
as-built O	Ni(K) at.%	50.3	49.7	49.8	47.9	49.3	49.4	0.9	7.822
	Mn(K) at.%	22.3	22.8	22.5	22.6	22.6	22.6	0.2	
	Ga(K) at.%	20.5	20.7	21.1	21.2	21.2	20.9	0.3	
	Co(K) at.%	3.3	3.2	3.3	3.2	3.2	3.2	0.1	
	Cu(K) at.%	3.6	3.6	3.3	3.4	3.7	3.5	0.2	

and O materials even in the as-built state. Fig. 4 demonstrates high-energy X-ray diffraction patterns of N and O samples in as-built and annealed states.

As was mentioned before, the samples directly after the LPBF process show a full martensite structure with peaks indexed in accordance with NM phase. The heat treatment temperature and time do not cause structural evolution. Nevertheless, the heat treatment released the internal stresses introduced during 3D printing process which is evidenced by straight peaks for alloys annealed at 900°C. Thus, it can be stated that chemically homogenous samples, with the desired structure were produced, thus, the heat treatment process was applied to release the internal stresses and improve microstructural homogeneity rather than change the structure. Generally, it is well known that the stability of martensite phases is correlated with their chemical composition, more precisely, electron valence concentration (e/a). Lanska et al. reported the critical values of e/a for each 10M, 14NM and NM structures. The electron concentration range for ternary Ni-Mn-Ga alloys with NM phase is from e/a = 7.61 to 7.82 with martensitic transformation temperature range of 50-277°C [28]. The calculated values of e/a are presented in TABLE 1 while being in the reported electronic concentration range.

TEM observations performed on N sample reveal the existence of fine nano twins with a width ranging between a dozen and several dozen nanometers. Fig. 5 presents the set of BF, DF and SADP images of N alloys. DF TEM images were carried out from reflections marked by red/green circles in the SADP image.

Additionally, complete pole figures were recorded by high-energy X-ray diffraction to evaluate the global texture of 3D printings and determine MFIS value. Fig. 6 demonstrates (004), (400) and (202) pole figures for as-built N and O alloys as well as for N samples annealed at 900°C/72 h before and after applying a magnetic field. Both alloys O and N reveal strong {100} texture along the growth direction, which was also shown in the case of ternary NiMnGa alloys in our previous work [26]. However, as can be seen, two components can be distinguished for O material, which is connected with the oscillating scanning strategy leading to the growth of columnar grains along the growth direction with a deviation of about two directions. The zigzag laser path causes dragging of the molten alloy along two directions In this point, it should be mentioned that texture analysis are in good agreement with microstructural observations.

Based on the pole figures recorded before and after applying the magnetic field (perpendicularly to the lateral surface), using the equation

$$e_{MFIS} = \left(1 - \frac{c}{a}\right) \cdot V_{fiber} \cdot V_C$$

where c and a are lattice parameters of martensite (NM), V_{fiber} and V_C are volume fraction of <100> fiber and volume fraction

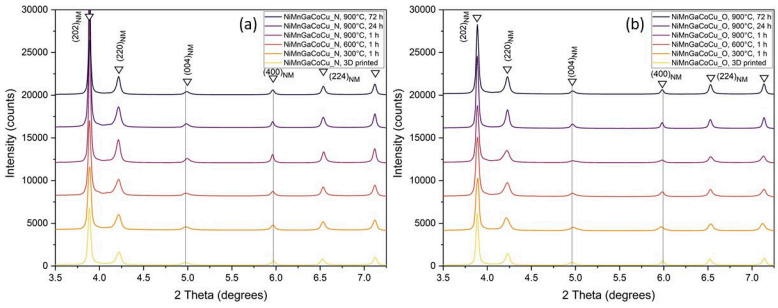

Fig. 4. High energy X-ray diffraction patterns of as-built and heat-treated N and O samples

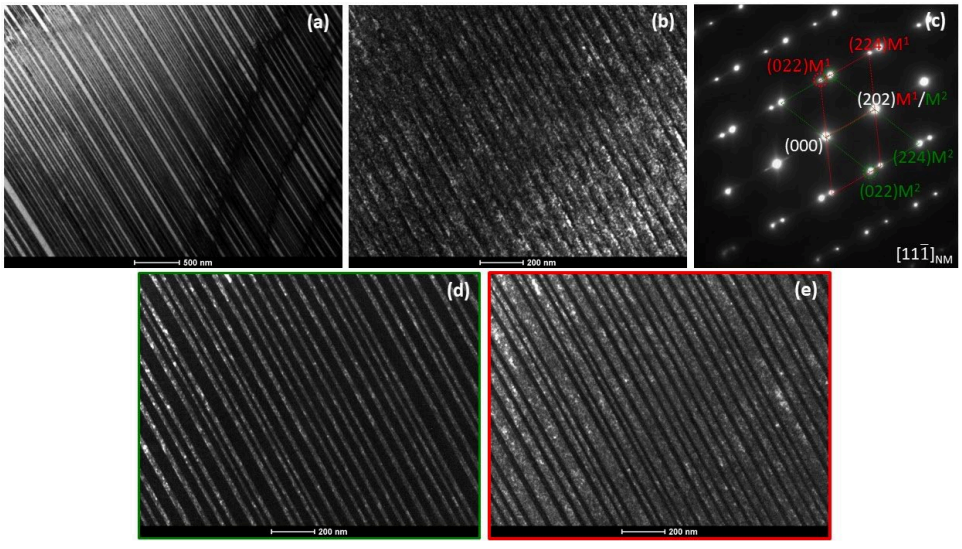

Fig. 5. BF TEM images (a), (b), corresponding SADP (c) and DF TEM mages recorded from two marked by circles points

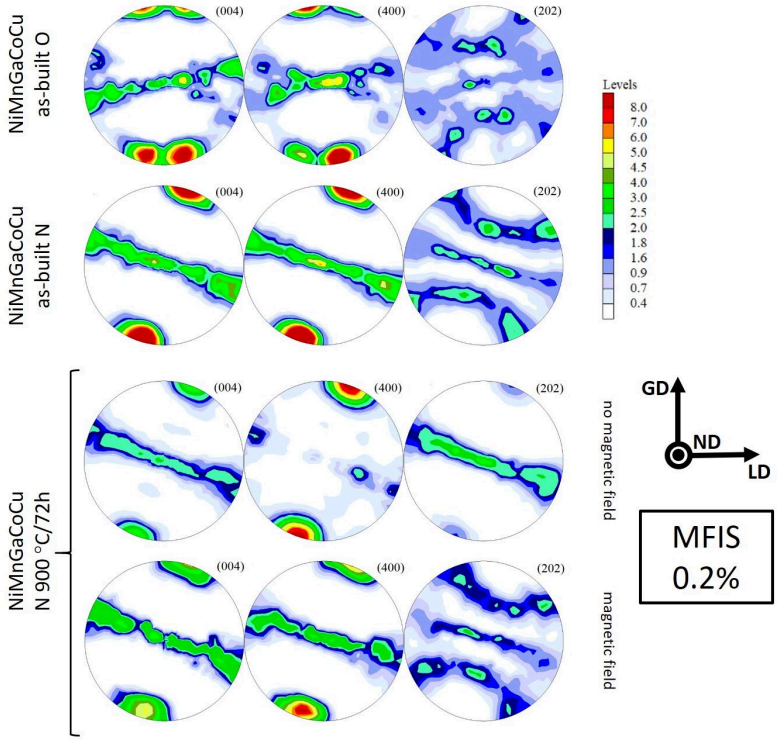

Fig. 6. Complete (004), (400) and (202) pole figures for as-built N and O samples and an alloy annealed at 900°C/72 recorded before and after applying a magnetic field

of variant reoriented when applied magnetic field, respectively [24,26], MFIS for the sample annealed at 900°C/72 h was calculated. The obtained value is 0.2% for the non-modulated structure which is slightly lower compared to 14M structure. The MFIS value was calculated only for annealed alloy which shows the highest chemical and microstructural homogeneity as well as the most atomically ordered structure.

Finally, the martensitic transformation and magnetic transition have been investigated using PPMS measurements. Curves recorded uder magnetic field of 500 Oe during cooling and heating (marked by arrows) are presented in Fig. 7. When cooling, the N and O as-bulit alloys show the rise of magnetization around 345 and 315K connected with the magnetic transition

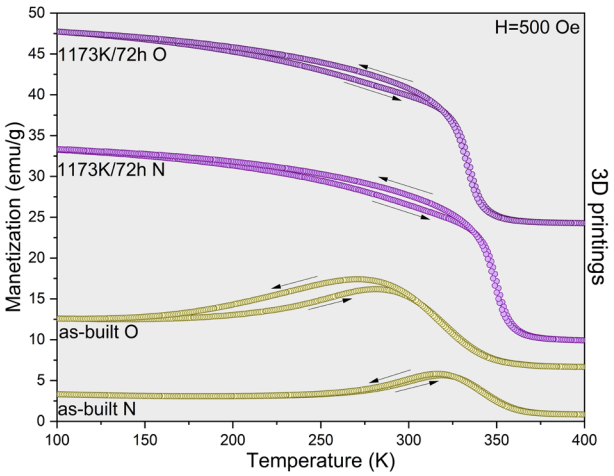

Fig 7. M(T) curves were recorded at magnetic field of 500 Oe during cooling and heating of N and O samples in as-built and annealed states

from paramagnetic to ferromagnetic austenite. Then, further drop of magnetization corresponds to martensitic transformation from high temperature parent austenite to low temperature martensite while the curves recorded during heating showing the increase of magnetization refer to reverse martensitic transformation. In the case of annealed alloys, the magnetization change at higher temperatures is related to magnetic transition of austenite while hysteresis loop (without significant magnetization change) below magnetic transition is connected with martensitic transformation. In all cases, the martensitic transformations show rather extended character which may be attributed to intermartensitic transformation from one type martensite.

The increase of martensitic transformation temperature with the increase of annealing temperature is related mainly to the internal stresses release and increase of atomic order degree of parent phase.

4. Conclusions

In this work, the microstructure and functional properties of NiMnGaCoCu 3D printings have been deeply investigated. The samples in as-built state, independently of the scanning strategy, show full martensite structure at room temperature indexed in accordance to tetragonal non-modulated structure while annealing does not affect the structure of the materials. The alloys were microstructurally and chemically homogenous even directly after 3D printing process. Interestingly, two regions with various morphological features and orientations of martensite variants have been found independently of the

scanning strategy. The calculated value of MFIS for non-modulated printed NiMnGaCoCu alloy after heat treatment was found to be 0.2%.

Acknowledgement

The work was financed by the Institute of Metallurgy and Materials Science of the Polish Academy of Sciences within the statutory work Z-12/2024 and the project 2021/42/E/ST5/00367 of the National Science Centre of Poland. The results were presented during 14th Polish Japanese Joint Seminar on Micro and Nano Analysis (3-6.09.2024, Toyama, Japan). The financial support of Polish Academy of Sciences is greatly appreciated.

REFERENCES

[1] P. Shah, R. Racasan, P.L. Bills, Comparison of different additive manufacturing methods using computed tomography. Case Studies in Nondestructive Testing and Evaluation **6**, 69-78 (2016).

[2] M. Attaran, The rise of 3-D printing: The advantages of additive manufacturing over traditional manufacturing. Business Horizons **60**, 677-688 (2017).

[3] M. Perez, D. Carou, E.M. Rubio, R. Teti, Current advances in additive manufacturing. Procedia CIRP **88**, 439-444 (2020).

[4] K.V. Wong, A. Hernandez, A review of Additive Manufacturing. ISRN Mechanical Engineering 208760 (2012).

[5] W.E. Frazier, Metal Additive Manufacturing: A Review. Journal of Materials Engineering and Performance **23**, 917-1928 (2014).

[6] V. Laitinen, A. Sozinov, A. Saren, A. Salminen, K. Ullakko, Laser powder bed fusion of NiMnGa magnetic shape memory alloy. Addit. Manuf. **30**, 100891 (2019).

[7] J. Toman, D.C. Pagan, P. Müllner, M. Chmielus, Epitaxial re-solidification of laser-melted NiMnGa single crystal. Acta Mater. **219**, 117236 (2021).

[8] V. Laitinen, A. Sozinov, A. Saren, M. Chmielus, K. Ullakko, Characterization of as-built and heat-treated NiMnGa magnetic shape memory alloy manufactured via laser powder bed fusion. Addit. Manuf. **39**, 101854 (2021).

[9] V. Laitinen, A. Saren, A. Sozinov, K. Ullakko, Giant 5.8% magnetic-field-induced strain in additive manufactured NiMnGa magnetic shape memory alloy. Scri. Mater. **208**, 114324 (2022).

[10] V.A. Chernenko, S. Besseghini, Ferromagnetic shape memory alloys: scientific and applied aspects. Sens. Actuators A **142** (2), 542 (2008).

[11] Y. Ezer, A. Sozinov, G. Kimmel, V. Etaleaniemi, N. Glavatskaya, A. D'Anci, V. Podgursky, V. Lindroos, K. Ullakko, Magnetic shape memory (MSM) effect in textured polycrystalline Ni_2MnGa. Smart. Struc. Mater. **3675**, 244 (1999).

[12] A. Sozinov, A.A. Likhachev, N. Lanska, K. Ullakko, Giant magnetic-field-induced strain in NiMnGa seven-layered martensitic phase. Appl. Phys. Lett. **80** (10),1746 (2002).

[13] K. Ullakko, J.K. Huang, C. Kantner, R.C.O'Handley, V.V. Kokorin, Large magnetic field-induced strains in Ni_2MnGa single crystals. Appl. Phys. Lett. **69**, 1966 (1996).

[14] P. Müllner, Twinning stress of type I and type II deformation twins. Acta Mater. **176**, 211-219 (2019).

[15] A. Sozinov, N. Lanska, A. Soroka, L. Straka, Highly mobile type II twin boundary in NiMnGa five-layered martensite. Appl. Phys. Lett. **99** (2011).

[16] L. Straka, O. Heczko, H. Seiner, N. Lanska, J. Drahokoupil, A. Soroka, S. Fahler, H. Hanninen, A. Sozinov, Highly mobile twinned interface in 10M modulated NiMn-Ga martensite. Acta Mater. **59**, 7450-7463 (2011).

[17] U. Gaitzsch, S. Roth, B. Rellinghaus, L. Schultz, Adjusting the crystal structure of NiMnGa shape memory ferromagnets. J. Magn. Magn. Mater. **305**, 275 (2006).

[18] U. Gaitzsch, J. Romberg, M. Pötschke, S. Roth, P. Müllner, Stable magnetic-field-induced strain above 1% in polycrystalline Ni–Mn–Ga. Scr. Mater. **65**, 679 (2011).

[19] M. Pötschke, U. Gaitzsch, S. Roth, B. Rellinghaus, L. Schultz, Preparation of melt textured Ni–Mn–Ga. J. Magn. Magn. Mater. **316**, 383 (2007).

[20] K. Ullakko, Y. Ezer, A. Sozinov, G. Kimmel, P. Yakovenko, V. Lindroos, Magnetic-field-induced strains in polycrystalline NiMnGa at room temperature. Scr. Mater. **44**, 475 (2001).

[21] U. Gaitzsch, M. Pötschke, S. Roth, B. Rellinghaus, L. Schultz, A 1% magnetostrain in polycrystalline 5M Ni–Mn–Ga. Acta Mater. **57**, 365 (2009).

[22] C. Hürrich, S. Roth, H. Wendrock, M. Pötschke, D. Cong, B. Rellinghaus, L. Schultz, Influence of grain size and training temperature on strain of polycrystalline $Ni_{50}Mn_{29}Ga_{21}$ samples. J. Phys. Conf. Ser. **303**, 012080 (2011).

[23] A. Wójcik, R. Chulist, P. Czaja, M. Kowalczyk, P. Zackiewicz, N. Schell, W. Maziarz, Evolution of microstructure and crystallographic texture of NiMnGa melt-spun ribbons exhibiting 1.15% magnetic field-induced strain. Acta Materialia **219**, 117237 (2021).

[24] W. Maziarz, P. Czaja, R. Chulist, A Wójcik, Ł. Żrodowski, B. Morończyk, R. Wróblewski, M. Kowalczyk, Microstructure and Magnetic Properties of Selected Laser Melted NiMnGa and NiMnGa-Fe Powders Derived from as Melt-Spun Ribbons Precursors. Metals **11**, 903 (2021).

[25] P. Czaja, R. Chulist, A. Wójcik, M. Kowalczyk, P. Zackiewicz, A. Szewczyk, N. Schell, W. Maziarz, Suppression and Recovery of Martensitic Transformation and Magnetism in Mechanically and Thermally Treated Magnetic Shape-Memory Ni−Mn−Ga Melt-Spun Ribbons. Adv. Eng. Mater. 2100075 (2021).

[26] A. Wojcik, R. Chulist, A. Szewczyk, B. Moronczyk, Ł. Zrodowski, R. Wroblewski, M. Kowalczyk, A. Kolano-Burian, P. Zackiewicz, N. Schell, W. Maziarz; Microstructure and texture control of Ni-Mn-Ga magnetic shape memory alloys manufactured by laser powder bed fusion. Additive Manufacturing **86**, 104225 (2024).

[27] R. Chulist, A. Wójcik, A. Sozinov, T. Tokarski, M. Faryna, N. Schell, W. Skrotzki, B. Li, H. Sehitoglu, X. Li, W. Maziarz, Adaptive Phase or Variant Formation at the Austenite/Twinned Martensite Interface in Modulated Ni–Mn–Ga Martensite. Advanced Fuctional Materials **34**, 2307322 (2024).

[28] N. Lanska, O. Soderberg, A. Sozinov, Y. Ge, K. Ullakko, V.K. Lindroos, Composition and temperature dependence of the crystal structure of Ni-Mn-Ga alloys, J. Appl. Phys. **95**, 8074 (2004).